

LETTERS

Spontaneous vortices in the formation of Bose–Einstein condensates

Chad N. Weiler¹, Tyler W. Neely¹, David R. Scherer¹, Ashton S. Bradley^{2†}, Matthew J. Davis² & Brian P. Anderson¹

Phase transitions are ubiquitous in nature, and can be arranged into universality classes such that systems having unrelated microscopic physics show identical scaling behaviour near the critical point. One prominent universal element of many continuous phase transitions is the spontaneous formation of topological defects during a quench through the critical point^{1–3}. The microscopic dynamics of defect formation in such transitions are generally difficult to investigate, particularly for superfluids^{4–7}. However, Bose–Einstein condensates (BECs) offer unique experimental and theoretical opportunities for probing these details. Here we present an experimental and theoretical study of the BEC phase transition of a trapped atomic gas, in which we observe and statistically characterize the spontaneous formation of vortices during condensation^{8,9}. Using microscopic theories^{10–17} that incorporate atomic interactions and quantum and thermal fluctuations of a finite-temperature Bose gas, we simulate condensation and observe vortex formation in close quantitative agreement with our experimental results. Our studies provide further understanding of the development of coherence in superfluids, and may allow for direct investigation of universal phase transition dynamics.

Spontaneous vortex formation in superfluids is intimately connected to superfluid growth. In one model, illustrated in Fig. 1, isolated superfluid regions of characteristic size ξ independently form as the system nears the critical point of the phase transition. These regions with random relative phases merge together during the transition, leading to a continuous phase gradient in the merged fluid. Owing to continuity requirements on the wavefunction, the merging process may trap phase loops of 2π if the merging regions have

suitable relative phases, as illustrated in Fig. 1. The superfluid density at the centre of these 2π phase loops is topologically constrained to be zero, resulting in the formation of a quantized vortex; the absence of superfluid at the vortex core may be viewed as arising from destructive interference between merging regions. Although cast here in the context of superfluid growth, spontaneous topological defect formation is a fundamental component of the Kibble–Zurek mechanism^{1–3}. Based on universality classes for second-order phase transitions, this mechanism provides a prescription for estimating a correlation length ξ and hence the density of defects, proportional to $1/\xi^2$, that may form. For a continuous phase transition that proceeds quasi-statically, ξ diverges at the critical point and therefore no defects are expected. However, in the Kibble–Zurek mechanism the phase transition occurs over a finite time, and the system falls out of equilibrium when the thermalization (or relaxation) rate drops below a quench rate $1/\tau_Q$. At this point ξ is frozen in and essentially remains constant through the critical point. A principal result is that faster quenches lead to an earlier freeze-in time, and hence smaller values of ξ and higher defect densities.

The Kibble–Zurek mechanism is appealing because of its potential for characterizing a wide variety of phase transitions, irrespective of the microscopic processes involved. A model of condensation in a homogeneous Bose gas describing the transition from a weak-turbulent (kinetic) stage to strong-turbulent (coherent) state has been proposed by Svistunov and co-workers^{9,18–21}. In this scheme, as energy is removed from the system the low-energy atomic field modes become macroscopically occupied. Destructive interference between these essentially classical modes leads to nodes in the field, which appear as lines of zero atomic density. Subsequently, a quasi-condensate having local coherence but no long-range coherence grows around the lines of zero density, which simultaneously evolve into well-structured vortex cores. Eventually the superfluid relaxes into equilibrium and a true condensate with global phase coherence is achieved. Berloff and Svistunov numerically demonstrated the validity of this picture for the homogeneous Bose gas in simulations of the Gross–Pitaevskii equation²² (see Supplementary Information). Our work involves an experimental and theoretical exploration of similar phenomena in the condensation of trapped gases. Our approach also has the potential to investigate the relationship of the Kibble–Zurek mechanism to phase transition dynamics of BECs.

In previous work we demonstrated that vortices can form during the controlled merging of three independent BECs with uncorrelated phases²³, an analogue of the Kibble–Zurek mechanism. Here we study vortex formation by evaporatively cooling an atomic gas through the BEC phase transition in a single axially symmetric oblate harmonic trap (see Methods). To probe condensate growth dynamics under varying cooling conditions, we use two temperature quenches: quench A uses a 6-s radiofrequency evaporative cooling

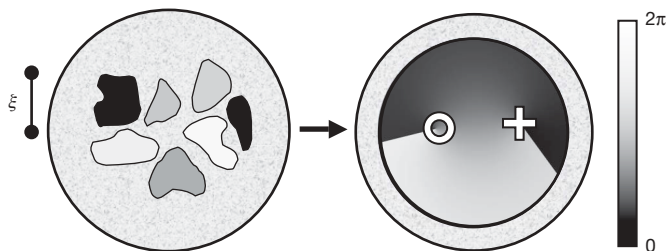


Figure 1 | Schematic of spontaneous vortex formation. Left, as a thermal gas (mottled grey) is cooled through the BEC transition, isolated coherent regions of approximate size ξ and unpredictable phase may form^{8,9}. Quantum phase ranges from 0 to 2π , represented here by shades of grey as indicated by the gradient bar at the right. Right, initial coherent regions eventually merge to form a single BEC (continuous greyscale region), potentially forming quantized vortices. Here, a positive (negative) vortex is labelled with a cross (circle), with the phase winding direction corresponding to the direction of superfluid flow and phase gradient about the vortex core.

¹College of Optical Sciences, University of Arizona, Tucson, Arizona 85721, USA. ²ARC Centre of Excellence for Quantum-Atom Optics, School of Physical Sciences, University of Queensland, Brisbane, Queensland 4072, Australia. †Present address: Jack Dodd Centre for Quantum Technology, Department of Physics, University of Otago, PO Box 56, Dunedin, New Zealand.

ramp, and quench B uses a sudden jump to a final radiofrequency value (see Methods). Plots of temperature and condensate number versus time for both quenches are shown in Fig. 2a. Following Anglin and Zurek⁸ (see Supplementary Information), we estimate a correlation length of $\xi \approx 0.6 \mu\text{m}$ near the critical point for both quenches. Because ξ is about a factor of 6 smaller than our radial harmonic oscillator length $a_r \approx 3.8 \mu\text{m}$ characterizing a condensate radius for small atom numbers, we would not expect global phase coherence at the critical temperature, suggesting that spontaneous vortex formation could occur in our experiments.

To look for vortices, we suddenly remove the trapping potential after the 6-s evaporative cooling ramp of quench A or 1.5 s after the radiofrequency jump for quench B. Each BEC ballistically expands and is then imaged along the vertical direction (the z axis), which coincides with the symmetry axis of the trap. Vortex cores aligned with the z axis appear as holes in the column-density distribution, as shown in Fig. 3a. We emphasize that our procedure does not impart net angular momentum to the atomic cloud, such as through phase engineering²⁴ or stirring²⁵; our observations thus represent a new regime for the study of quantized vortex nucleation in BECs (see Supplementary Information for further discussion).

We simulate condensate formation using the stochastic Gross–Pitaevskii equation (SGPE) formalism^{13,14} that describes the highly occupied, low-energy modes of a Bose gas with a classical field. The field evolves according to a generalized Gross–Pitaevskii equation that includes dissipation and thermal noise describing collisions between the partially condensed matter waves and the high-energy atoms in the thermal cloud. Because evaporative cooling is difficult to simulate realistically²⁶, and the details are often qualitatively

unimportant, we use an idealized cooling model with a sudden jump in chemical potential and temperature of the thermal cloud through the condensation critical point. This leaves the SGPE classical field out of equilibrium with the thermal cloud; the subsequent return to equilibrium results in condensate formation. Figure 2a shows the growth in condensate number for the simulations of both quenches. In our simulations, the initial and final thermal cloud parameters have been chosen to match the experimental results, and the coupling between the thermal cloud and the classical field is then adjusted to give good agreement with the experimentally observed BEC growth curves. This approach allows a meaningful comparison of other observables such as vortex statistics with the experimental data. Further discussion can be found in the Methods and Supplementary Information.

As shown in Fig. 3b, c, vortices spontaneously form in our simulations, where each realization can be interpreted as the numerical analogue of a single experimental run. We therefore study vortex dynamics in each growing condensate to compare vortex formation statistics with our experimental results. In both our laboratory and numerical procedures, for each quench we repeat the BEC creation procedure and analyse statistics of vortex observations. For each data set described below, we extract the fraction of images showing at least one vortex core within a displacement of $0.8R_{\text{TF}}$ from the BEC centre, where R_{TF} is the BEC Thomas–Fermi radius in the $z = 0$ plane²⁷. This fraction serves as our estimate of the probability of observing spontaneously formed vortices in a single run.

Because localized decreases in the density profile of an experimentally obtained image may not always clearly indicate the presence of a core (for example, owing to tilting or bending with respect to the z axis) our experimental uncertainty ranges are defined by our ability to determine visually whether an image shows a vortex. For quench A, 23–28% of 90 total images contain at least one visible vortex core. For quench B, 15–20% of 98 total images show at least one core. Although the two quenches use quite different radiofrequency evaporation trajectories, they show similar cooling and BEC growth rates. We can thus expect statistical similarities between the two data sets. Further statistical details, including results of observing multiple cores per image, are given in the Supplementary Information.

From our simulations, we can analyse vortex observation probabilities as a function of time for each quench. To determine the presence of a vortex we consider an instantaneous slice of the classical field in the $z = 0$ plane of the trap, and detect all phase loops of $\pm 2\pi$ within a displacement of $0.8R_{\text{TF}}$ from the BEC centre (here, R_{TF} is based on the time-dependent condensate number). We find that the

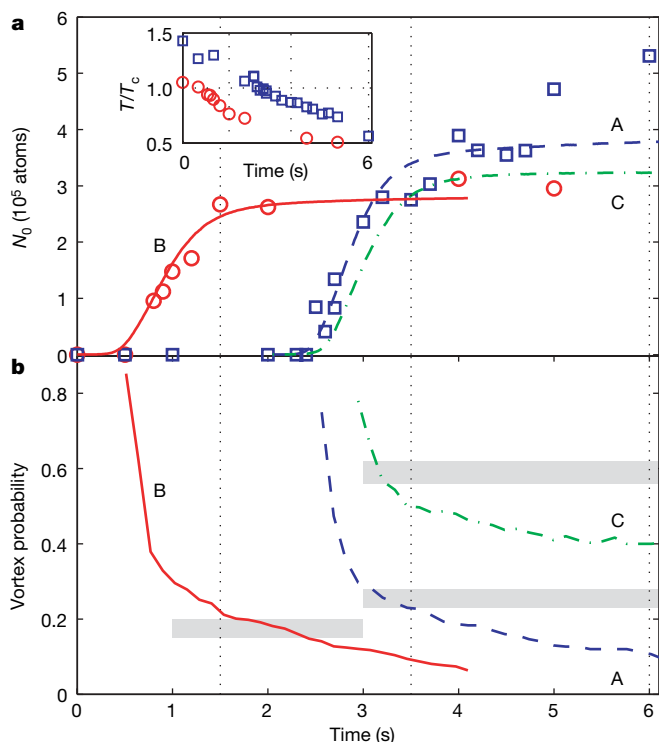


Figure 2 | Condensate formation and vorticity. **a**, Condensate number N_0 versus time. Blue squares (red circles) indicate experimental data for quench A (B), and lines indicate corresponding numerical simulations. The green dot-dashed line is the numerical result for the toroidal trap (quench C). Vertical dotted lines indicate the observation times for which experimental statistics are generated. Inset, experimentally measured temperatures for quenches A and B ($\tau_Q \approx 7$ s and 5 s, respectively). **b**, The probability of finding at least one vortex passing through the $z = 0$ plane plotted for all three simulated quenches. Grey regions indicate the experimental measurement range for each data set.

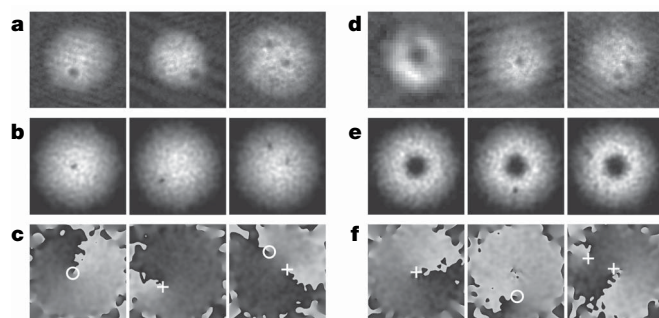


Figure 3 | Vortices in the harmonic and toroidal traps. **a**, Images of BECs created in a harmonic trap, showing single vortices (left, centre) and two vortices (right). Each image is $200 \mu\text{m}$ square. **b**, **c**, Sample simulation results from quench B, showing in-trap integrated column densities along z (in **b**) and associated phase profiles in the $z = 0$ plane (in **c**), with vortices indicated by crosses and circles at $\pm 2\pi$ phase windings. **d**, Left image, phase-contrast experimental image of a BEC in the toroidal trap. Image is $70 \mu\text{m}$ square. Remaining images, vortices in $200\text{-}\mu\text{m}$ -square expansion images of BECs created in the toroidal trap. **e**, **f**, Simulations of BEC growth in the toroidal trap show vortices (as in **b**, **c**) and persistent currents.

majority of vortices are aligned with the z axis of the trap. The vortex observation probabilities obtained from ~ 300 simulation runs for each quench are plotted against time in Fig. 2b, with comparison to the experimental statistics.

According to our simulations, the number of vortices decreases with time, consistent with our model of a thermal bath that is independent of time and has no angular momentum; the thermodynamic final state should therefore be a condensate without vortices. In this respect the simulations diverge from our experimental observations, where there is no significant variation of vortex observation probabilities over a timescale of a few seconds. This low damping rate is consistent with the comparatively small thermal component observed, indicating that a kinetic theory of thermal cloud dynamics may be needed to account fully for the long-time behaviour of the experiment. We therefore compare our simulation results at $t = 3.5$ s for quench A, and $t = 1.5$ s for quench B, based on experimental observations of negligible vortex damping once the BEC is nearly fully formed.

By focusing a blue-detuned laser beam propagating along the z axis into the centre of the trap (see Methods), we experimentally studied BEC growth in a toroidal potential in which a BEC may display both persistent superfluid current²⁸ about the central barrier as well as free vortices circulating around the barrier. The pinning of superfluid flow may influence both vortex dynamics during BEC growth and observations of vortices after the BEC is formed: a vortex pinned to the barrier reduces the likelihood of complete self-annihilation between pairs of spontaneously formed vortices of opposite charge, thereby increasing the probability of finding a vortex in a BEC. We apply a 6-s final evaporative cooling ramp identical to quench A, and identify this data set as quench C. An *in situ* image of a BEC in the toroidal trap is given in the leftmost image of Fig. 3d. Note that the dark region in the BEC centre indicates atoms displaced by the laser beam; vortices are not visible in this image. After creating each BEC, we ramp down the laser power over 100 ms and immediately thereafter allow the BEC to expand from the trapping potential. For these conditions, we find that 56–62% of 52 images contained at least one visible core; examples are shown in Fig. 3d.

Condensate formation rates were not experimentally measured for quench C; for the simulations we use the parameters of quench A but with an additional repulsive Gaussian barrier. Simulated condensate growth versus time resulted in smaller condensates than for quench A (also observed experimentally) as shown by the green dot-dashed curve in Fig. 2a. Examples of numerically obtained column density and phase are shown in Fig. 3e, f. Vortex observation statistics for 300 runs are plotted as a green dot-dashed line in Fig. 2b; we find that the vortex observation probability is about twice that of the harmonic trap of quench A, as is also the case with the experimental data, but is somewhat lower in overall magnitude than the experimental observations. In contrast to the harmonic case, the curve does not show decay below 40%, which corresponds to the fraction of runs with vortices pinned by the Gaussian potential. This potential provides a sufficient energy barrier to prevent the condensate from reaching its thermodynamic ground state with zero angular momentum despite the presence of dissipation. Moreover, it is likely that vortex pinning by the Gaussian barrier is the physical mechanism responsible for the overall increase in the probability of observing vortices in the toroidal case as compared with the harmonic case. Additional toroidal trap statistics are provided in the Supplementary Information.

In the Supplementary Information, we provide movies of simulated condensate formation for quenches A and C. Here we describe one run in which a single vortex persists to the end of a quench A simulation in the harmonic trap. After the system temperature is initially lowered, the atomic density fluctuates temporally and spatially, as illustrated in Fig. 4a. A bulk BEC then begins to grow, and a tangle of vortices is trapped within the BEC as shown in Fig. 4b, in qualitative agreement with the models of superfluid turbulence^{9,18–22} and the Kibble–Zurek mechanism^{1–3,8}. The condensate now forms rapidly, but with clear vortex cores as shown in Fig. 4c. This state eventually damps to a single core as seen in Fig. 4d.

In examining the relationship between the BEC transition and the Kibble–Zurek mechanism, one would ideally study vortex formation with widely varying BEC growth rates in order to test the predictions of the scaling of the vortex density^{1–3}. However, in our harmonic traps, we have only succeeded in increasing BEC growth rates by a

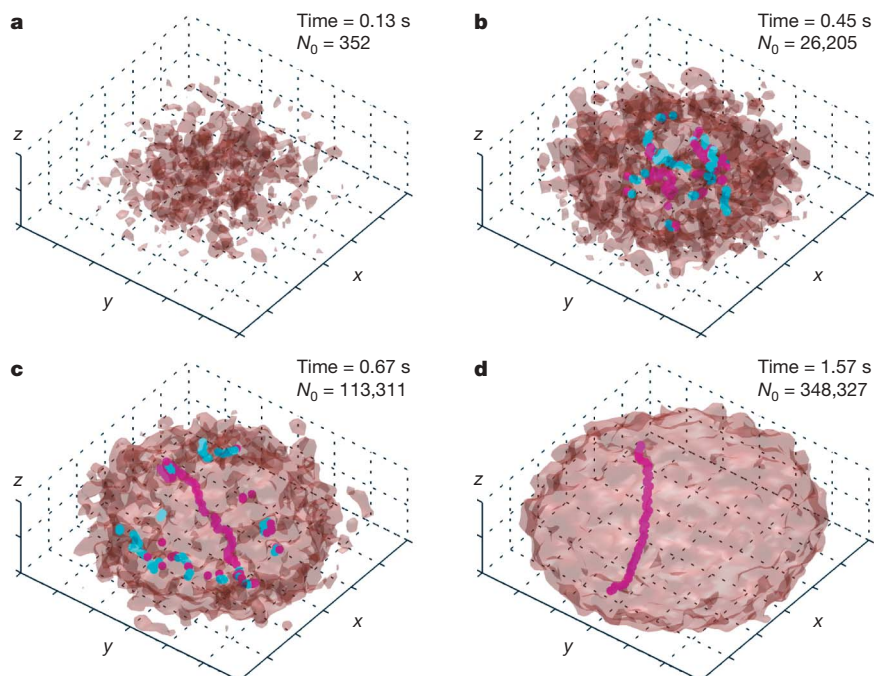


Figure 4 | BEC growth dynamics. a–d, Four snapshots during the simulated growth of a BEC showing isodensity surfaces (in light red) in a three-dimensional rendering. Vortex cores of opposite charges about the z axis are indicated as magenta and cyan lines. The corresponding times are 0.13 s (a),

0.45 s (b), 0.67 s (c), 1.57 s (d), where $t = 0$ s is the time when the quench is initiated in the simulation. The full movie from which these images were taken is provided as Supplementary Video 3.

factor of two to three, resulting in a factor of ~ 2 increase in vortex formation compared with quenches A and B. In simulations, faster growth rates can potentially result in more vortices, as discussed in the Supplementary Information.

In addition to providing new experimental observations, our work places spontaneous topological defect formation on a theoretical foundation that has not been available in analogous studies in other systems. Related experimental investigations of spontaneous symmetry breaking of quenched ferromagnetic spinor BECs²⁹ may also yield insight into phase transition dynamics. The quantitative agreement between our experimental and theoretical results is of primary importance for their mutual interpretation: even in the ultra-cold BEC phase transition, thermal fluctuations can have an important role, and spontaneous topological defect formation may be virtually unavoidable in some situations. Our continuing work will explore in greater detail exactly how a condensate forms in this regime; the superfluid turbulence model describes vortex formation during condensation, but to what extent does the Kibble–Zurek mechanism's universality relate to the BEC transition? With further simulations and experiments, new details of the development of coherence in the birth of a superfluid may be uncovered, a tantalizing prospect addressing the interface between the classical and quantum worlds.

METHODS SUMMARY

In our experiments, ⁸⁷Rb atoms in the $|F=1, m_F=-1\rangle$ hyperfine state are confined in a time-averaged orbiting potential magnetic trap³⁰. Evaporative cooling increases the phase space density to near the condensation critical point. The trap frequencies are then relaxed, and a final stage of cooling (quench A, B or C) induces the phase transition. In our numerical approach we describe the evolution of the condensate and its highly occupied excitations using a stochastic Gross–Pitaevskii equation coupled to a thermal reservoir parameterized by a chemical potential μ and temperature T initially above the critical point. Evaporative cooling is simulated by a sudden change in μ and T . Further details regarding our approaches are provided in the full Methods.

Full Methods and any associated references are available in the online version of the paper at www.nature.com/nature.

Received 28 March; accepted 12 August 2008.

1. Kibble, T. W. B. Topology of cosmic domains and strings. *J. Phys. A* **9**, 1387–1398 (1976).
2. Zurek, W. H. Cosmological experiments in superfluid helium? *Nature* **317**, 505–508 (1985).
3. Zurek, W. H. Cosmological experiments in condensed matter systems. *Phys. Rep.* **276**, 177–221 (1996).
4. Hendry, P. C., Lawson, N. S., Lee, R., McClintock, P. V. E. & Williams, C. D. H. Generation of defects in superfluid ⁴He as an analogue of the formation of cosmic strings. *Nature* **368**, 315–317 (1994).
5. Ruutu, V. M. H. *et al.* Vortex formation in neutron-irradiated superfluid ³He as an analogue of cosmological defect formation. *Nature* **382**, 334–336 (1996).
6. Bäuerle, C., Bunkov, Y. M., Fisher, S. N., Godfrin, H. & Pickett, G. R. Laboratory simulation of cosmic string formation in the early Universe using superfluid ³He. *Nature* **382**, 332–334 (1996).
7. Dodd, M., Hendry, P., Lawson, N., McClintock, P. & Williams, C. Nonappearance of vortices in the fast mechanical expansions of liquid ⁴He through the Lambda transition. *Phys. Rev. Lett.* **81**, 3703–3706 (1998).
8. Anglin, J. R. & Zurek, W. H. Vortices in the wake of rapid Bose–Einstein condensation. *Phys. Rev. Lett.* **83**, 1707–1710 (1999).

9. Svistunov, B. V. Strongly non-equilibrium Bose–Einstein condensation in a trapped gas. *Phys. Lett. A* **287**, 169–174 (2001).
10. Stoof, H. T. C. Coherent versus incoherent dynamics during Bose–Einstein condensation in atomic gases. *J. Low Temp. Phys.* **114**, 11–108 (1999).
11. Davis, M. J., Ballagh, R. J. & Burnett, K. Dynamics of thermal Bose fields in the classical limit. *J. Phys. B* **34**, 4487–4512 (2001).
12. Davis, M. J., Morgan, S. A. & Burnett, K. Simulations of Bose fields at finite temperature. *Phys. Rev. Lett.* **87**, 160402 (2001).
13. Gardiner, C. W., Anglin, J. R. & Fudge, T. I. A. The stochastic Gross–Pitaevskii equation. *J. Phys. B* **35**, 1555–1582 (2002).
14. Gardiner, C. W. & Davis, M. J. The stochastic Gross–Pitaevskii equation: II. *J. Phys. B* **36**, 4731–4753 (2003).
15. Blakie, P. B. & Davis, M. J. Projected Gross–Pitaevskii equation for harmonically confined Bose gases at finite temperature. *Phys. Rev. A* **72**, 063608 (2005).
16. Davis, M. J. & Blakie, P. B. Critical temperature of a trapped Bose gas: Comparison of theory and experiment. *Phys. Rev. Lett.* **96**, 060404 (2006).
17. Bradley, A. S., Gardiner, C. W. & Davis, M. J. Bose–Einstein condensation from a rotating thermal cloud: Vortex nucleation and lattice formation. *Phys. Rev. A* **77**, 033616 (2008).
18. Svistunov, B. V. Highly nonequilibrium Bose condensation in a weakly interacting gas. *J. Mosc. Phys. Soc.* **1**, 373–390 (1991).
19. Kagan, Y., Svistunov, B. V. & Shlyapnikov, G. V. The Bose-condensation kinetics in an interacting Bose–gas. *Zh. Eksp. Teor. Fiz. [Sov. Phys. JETP]* **75**, 387 (1992)] **101**, 528–539 (1992).
20. Kagan, Y. & Svistunov, B. V. Kinetics of long-range order formation in Bose-condensation in interacting gas. *Zh. Eksp. Teor. Fiz. [Sov. Phys. JETP]* **78**, 187 (1994)] **105**, 353–367 (1994).
21. Kagan, Y. & Svistunov, B. V. Evolution of correlation properties and appearance of broken symmetry in the process of Bose–Einstein condensation. *Phys. Rev. Lett.* **79**, 3331–3334 (1997).
22. Berloff, N. G. & Svistunov, B. V. Scenario of strongly nonequilibrium Bose–Einstein condensation. *Phys. Rev. A* **66**, 013603 (2002).
23. Scherer, D. R., Weiler, C. N., Neely, T. W. & Anderson, B. P. Vortex formation by merging of multiple trapped Bose–Einstein condensates. *Phys. Rev. Lett.* **98**, 110402 (2007).
24. Matthews, M. R. *et al.* Vortices in a Bose–Einstein condensate. *Phys. Rev. Lett.* **83**, 2498–2501 (1999).
25. Madison, K. W., Chevy, F., Wohlleben, W. & Dalibard, J. Vortex formation in a stirred Bose–Einstein condensate. *Phys. Rev. Lett.* **84**, 806–809 (2000).
26. Davis, M. J. & Gardiner, C. W. Growth of a Bose–Einstein condensate: a detailed comparison of theory and experiment. *J. Phys. B* **35**, 733–742 (2002).
27. Pethick, C. & Smith, H. *Bose–Einstein Condensation in Dilute Gases* (Cambridge Univ. Press, 2002).
28. Ryu, C. *et al.* Observation of persistent flow of a Bose–Einstein condensate in a toroidal trap. *Phys. Rev. Lett.* **99**, 260401 (2007).
29. Sadler, L. E., Higbie, J. M., Leslie, S. R., Vengalattore, M. & Stamper-Kurn, D. M. Spontaneous symmetry breaking in a quenched ferromagnetic spinor Bose–Einstein condensate. *Nature* **443**, 312–315 (2006).
30. Petrich, W., Anderson, M., Ensher, J. & Cornell, E. Stable, tightly confining magnetic trap for evaporative cooling of neutral atoms. *Phys. Rev. Lett.* **74**, 3352–3355 (1995).

Supplementary Information is linked to the online version of the paper at www.nature.com/nature.

Acknowledgements We thank D. Roberts, B. Svistunov, E. Wright and W. Zurek for discussions. The experimental work was financially supported by the US National Science Foundation under grant no. 0354977, and by the Army Research Office. The theoretical work was financially supported by the Australian Research Council Centre of Excellence for Quantum-Atom Optics and the University of Queensland.

Author Information Reprints and permissions information is available at www.nature.com/reprints. Correspondence and requests for materials should be addressed to B.P.A. (bpa@optics.arizona.edu).

METHODS

Evaporative cooling. During the main evaporative cooling stages of our experimental procedure, our time-averaged orbiting potential (TOP) magnetic trap is created with a spherical quadrupole field that has a vertical magnetic field gradient of $B_z' = 300 \text{ G cm}^{-1}$, and a magnetic bias field B_0 that has a direction that rotates in a horizontal plane at a frequency of either $\omega_{\text{rot}} = 2\pi \times 4 \text{ kHz}$ or $\omega_{\text{rot}} = 2\pi \times 2 \text{ kHz}$. Evaporative cooling proceeds over 72 s as B_0 decreases from 41 G to $\sim 5.2 \text{ G}$, leaving a trapped cloud of atoms just above the condensation critical temperature T_c . The magnetic field gradient B_z' is then adiabatically reduced to $\sim 54 \text{ G cm}^{-1}$ over 2 s, weakening the harmonic oscillator trapping frequencies to a measured radial (horizontal) trapping frequency of $\omega_r = 2\pi \times 7.8(\pm 0.1) \text{ Hz}$ and an axial (vertical) trapping frequency of $\omega_z = 2\pi \times 15.3(\pm 0.2) \text{ Hz}$. The centre-of-mass position of the atom cloud correspondingly sags by about 0.6 mm vertically. In the final stage of our cooling cycle for quench A, we use a continuous 6-s ramp of the radiofrequency field, which evaporatively cools the atomic cloud from 70 nK to 20 nK, with $T_c \approx 42 \text{ nK}$, to create condensates of $N_c \approx 5 \times 10^5$ atoms. For quench B, the continuous radiofrequency evaporative cooling ramp is replaced with a sudden jump to a final radiofrequency value, followed by a hold of the atomic sample in the trap before release and imaging. In this situation we find $T_c \approx 35 \text{ nK}$ and the final condensate number is $N_c \approx 3 \times 10^5$ atoms.

TOP trap. To ensure that the rotating bias field of the TOP trap plays no significant role in the spontaneous formation of vortices, we measured the z component of the net orbital angular momentum L_z of our condensates using surface wave spectroscopy. We excite a quadrupolar oscillation of the BEC in the horizontal plane, and stroboscopically probe the BEC with a set of non-destructive in-trap phase-contrast images²⁷, obtained by probing along the z axis^{31,32}. The quadrupolar oscillations will then precess with a rate and direction proportional to L_z . In our measurements, there was no significant biasing of surface mode precession in a direction corresponding to the TOP trap rotation direction, an indication that TOP trap temporal dynamics have little to no influence on spontaneous vortex formation. This is discussed further in the Supplementary Information.

Toroidal trap. A potential-energy barrier was added to the centre of the magnetic trap using a focused blue-detuned laser beam with a wavelength of 660 nm, $\sim 18 \mu\text{W}$ of power, and a $\sim 6\text{-}\mu\text{m}$ Gaussian radius. The maximum beam intensity corresponds to a potential energy of roughly $k_B \times 20 \text{ nK}$, where k_B is Boltzmann's constant. This can be compared with a chemical potential of about $k_B \times 10 \text{ nK}$ for our fully formed BECs in the purely harmonic trap. The beam was adiabatically ramped on before the final 6-s evaporation ramp, only slightly perturbing the thermal cloud but providing enough additional potential energy to exclude BEC atoms from the z axis of the trap.

Imaging. Our main imaging procedure involves the sudden removal of the magnetic trap, and the subsequent ballistic expansion of the trapped cloud. After 59 ms of expansion in the presence of an additional magnetic field to support the atoms against gravity, the atomic cloud is illuminated with near-resonant laser light, and the absorption profile of the atomic density distribution is imaged onto a camera. In our greyscale images, lighter shades represent higher optical depth, proportional to integrated column density along the line of sight in the z direction. A clear vortex core aligned along the z axis appears as a dark hole in the density distribution.

Stochastic Gross–Pitaevskii theory. We denote the condensate and low-energy portion of the trapped gas with the field $\alpha(\mathbf{x}, t)$, and define the Gross–Pitaevskii operator

$$L_{\text{GP}} = -\frac{\hbar^2}{2m}\nabla^2 + V(\mathbf{x}) + g|\alpha(\mathbf{x}, t)|^2 \quad (1)$$

where m is the mass of an atom, $V(\mathbf{x})$ is the trapping potential, $g = 4\pi\hbar^2 a/m$ characterizes the strength of atomic interactions, and a is the s -wave scattering length. The equation of motion for the field is

$$d\alpha(\mathbf{x}, t) = \mathcal{P} \left\{ -\frac{i}{\hbar} L_{\text{GP}} \alpha(\mathbf{x}, t) dt + \frac{G(\mathbf{x})}{k_B T} (\mu - L_{\text{GP}}) \alpha(\mathbf{x}, t) dt + dW_G(\mathbf{x}, t) \right\} \quad (2)$$

which has been derived from first principles using the Wigner phase-space representation¹⁴. The first term on the right describes unitary evolution of the classical field according to the Gross–Pitaevskii equation. The second term represents growth processes, that is, collisions that transfer atoms from the thermal bath to the classical field and vice versa, and the form of $G(\mathbf{x})$ may be determined from kinetic theory¹⁷. The third term is the complex-valued noise associated with condensate growth. The noise has Gaussian statistics and is defined by its only non-vanishing moment: $\langle dW_G^*(\mathbf{x}, t) dW_G(\mathbf{x}', t') \rangle = 2G(\mathbf{x}) dt \delta(\mathbf{x} - \mathbf{x}') \delta(t - t')$; it is also consistent with the fluctuation-dissipation theorem. The projection operator \mathcal{P} restricts the dynamics to the low-energy region^{12,15} defined by all harmonic oscillator modes with energy $\epsilon < E_{\text{cut}} = 40\hbar\omega_r$ for these calculations, which for our parameters gives about three particles per mode at the cut-off. For typical experimental parameters this method is accurate from slightly above the critical temperature to colder temperatures where there is still a significant thermal fraction¹⁶.

The initial states used in our simulations are independent field configurations generated by ergodic evolution of the SGPE at equilibrium with the thermal cloud with $\mu_i = \hbar\omega_r$ and $T_i = 45$ (35) nK for quench A (B), representing the thermalized Bose gas above the transition temperature¹⁶. These parameters are then suddenly changed to final values chosen to match the final condensate number and temperature observed in the experiment: $\mu_f = 25$ (22) $\hbar\omega_r$ and $T_f = 34$ (25) nK for quench A (B). We perform simulations for 300 (298) sets of initial conditions. By averaging over the different realizations we can calculate any quantum mechanical observable as a function of time, and in particular we diagonalize the single-particle density matrix to find the number of atoms in the condensate¹⁵.

Because vortex formation is expected to depend on the BEC growth rate, which is difficult to calculate precisely, we adjust the coupling rate describing Bose-enhanced collisions between the classical field and thermal cloud to obtain a close match for the experimental BEC growth curves. We choose a spatially constant rate for the dimensionless coupling $\gamma = \hbar G(\mathbf{x})/k_B T$, shown to be a good approximation by Bradley *et al.*¹⁷. The noise at each time step then has the explicit form $dW_G(\mathbf{x}, t) = \sum \phi_j(\mathbf{x}) \sqrt{\gamma k_B T dt / \hbar} (\eta_j + i\zeta_j)$, where $\phi_j(\mathbf{x})$ are the single-particle modes below the cut-off and the real Gaussian variables η_j, ζ_j are independent and have zero mean and unit variance. In principle γ is specified by a quantum Boltzmann integral, but here we treat it as an experimental fitting parameter for the condensate growth rate; it is never more than a factor of two different from the result of Eq. (A11) in Bradley *et al.*¹⁷. The effect of these parameter choices is discussed further in the Supplementary Information.

31. Chevy, F., Madison, K. W. & Dalibard, J. Measurement of the angular momentum of a rotating Bose–Einstein condensate. *Phys. Rev. Lett.* **85**, 2223–2227 (2000).
32. Haljan, P. C., Anderson, B. P., Coddington, I. & Cornell, E. A. Use of surface-wave spectroscopy to characterize tilt modes of a vortex in a Bose–Einstein condensate. *Phys. Rev. Lett.* **86**, 2922–2925 (2001).